Nanomed. J. 7(1): 49-57, Winter 2020

RESEARCH PAPER

Comparison of the presence and non-presence states of magnetite nanoparticles in tissue-equivalent breast phantom via radiofrequency hyperthermia

Seyede Mahsa Kavousi [1], Seyed Erfan Saadatmand [1], Nader Riyahi Alam [1*], Seyed Rabi Mahdavi [2], Leila Khalafi [2]

[1]Department of Physics and Medical Engineering, School of Medicine, Tehran University of Medical Sciences (TUMS), Tehran, Iran
[2]Department of Physics and Medical Engineering, School of Medicine, Iran University of Medical Sciences, Tehran, Iran

ABSTRACT

Objective(s): Breast cancer is a fatal disease and the leading cause of mortality in women. Radiofrequency hyperthermia is an approach to the treatment of cancer cells through increasing their temperature. The present study aimed to investigate breast tumor ablation via radiofrequency hyperthermia in the presence and non-presence states of magnetite nanoparticles and assess the effects of magnetite nanoparticles on breast cancer treatment in hyperthermia.

Materials and Methods: Radius hemisphere geometry (5 cm) was designed, which was similar to an actual breast based on the fat tissues, glandular tissues as a semi-oval embedded in the hemisphere, and a radius sphere (1 cm) as a tumor region inside. After utilization in a three-dimensional printer, each layer of the phantom was filled with a proper combination of oil-gelatin with similar dielectric and thermal properties to an actual breast. To evaluate the effects of the magnetite nanoparticles, three weights of the magnetite were added to the tumor region (0.01, 0.05, and 0.1 g). Finally, the phantom was placed in a radiofrequency device with the frequency of 13.56 MHz.

Results: Temperature differences were measured at four different points of the phantom. The power and time in the treatment were estimated at 40 watts and five minutes, respectively. The temperature and specific absorption rate plots were obtained for all the states in several graphs for five minutes.

The results showed that the heat generation with the utilization of the magnetite state was higher by approximately 2.5-7˚C compared to the state without magnetite. Furthermore, the temperature of 0.05 gram of magnetite indicated that without causing damage in the healthy tissues, the entire tumor region could attain adequate heat uniformly (6.1-6.4˚C).

Conclusion: Therefore, it could be concluded that 0.05 gram of magnetite could cause ablation in the entire tumor region.

Keywords: *Breast Phantom, Magnetite Nanoparticles, Oil-gelatin Phantom, Radiofrequency Hyperthermia, Specific Absorption Rate (SAR)*

How to cite this article

Kavousi S M, Saadatmand S E, Riyahi Alam N, Mahdavi S R, Khalafi L. Comparison of the presence and non-presence states of magnetite nanoparticles in tissue-equivalent breast phantom via radiofrequency hyperthermia. Nanomed J. 2020; 7(1):49-57. DOI: 10.22038/nmj.2020.07.06

INTRODUCTION

Breast cancer is considered to be the most prevalent malignancy and the leading cause of mortality in women worldwide [1]. Despite the advancement in clinical therapy, treatment failure still occurs in the majority of breast cancer patients, and the mortality rate of the disease has been reported to be on the rise mainly due to an evolutionary process toward a metastatic and treatment-resistant disease [2-4].

Hyperthermia therapy involves the application of supra-normal body temperatures as an adjunct cancer treatment. This therapeutic approach has been investigated for several decades due to the relatively high thermal sensitivity of malignant cells compared to healthy tissues [5, 6]. Heat could be delivered using various techniques, such

* *Corresponding Author Email: riahialam@gmail.com*
Note. This manuscript was submitted on Setember 9, 2019; approved on November15, 2019

as radiofrequency, microwave radiation, regional perfusion therapy, laser ablation, and magnetic hyperthermia [7-9]. Recently, radiofrequency ablation has gained importance in the treatment of cancerous tumors. Hyperthermia is mostly identified based on the temperature range of 40-48°C or similar temperatures maintained at the treatment site for the duration of one hour or more [10-13]. The increased temperature could cause damage in tumor cells, while it is tolerated by normal tissues. Magnetic heat treatment is also considered to be an effective local, minimally invasive method for cancer treatment, which is associated with few or no adverse complications [14]. In 1957, Gilchrist suggested the use of magnetic particles for the increasing of local temperature in a target region as induced by an external magnetic field [15].

Hyperthermia has two prominent properties, which are referred to as the dielectric and thermal properties. Several studies have demonstrated the efficacy of magnetite nanoparticles in hyperthermia and breast cancer phantoms, while most of these studies have not considered both properties of this method simultaneously [16-18] or have failed to use proper geometry in the development of breast phantoms [19, 20]. In addition, some of these studies have not considered the glandular tissues of the breast [21] or have not utilized the phantom in experimental studies despite considering the mentioned factors [22]. Although the properties of magnetite nanoparticles that play a key role in hyperthermia treatment have been adequately investigated [23, 24], data is insufficient regarding the effects of these nanoparticles. In most of the studies in this regard, magnetite nanoparticles have been investigated in the fluid form, and their gel mixture has not been used [25-28].

Moreover, most of these studies have been focused on the frequency ranges that are not applied in the clinical treatments of breast cancer, no clinical devices have been utilized as the radiofrequency source. According to the literature [29], frequency is inversely proportional to the depth of penetration. At the frequency of 900 MHz, the body depth of 4.2 centimeters and frequencies above this level cannot be used for the treatment of breast tumors in clinical treatments. In a previous study in this regard, proper geometry was designed for breast, and a phantom was fabricated using an oil-gelatin mixture with similar thermal and dielectric properties to an actual breast. After determining the properties of the phantom, the phantom was placed in an electromagnetic field with the frequency of 13.56 MHz. Eventually, the thermal effects on the tissue-equivalent breast phantom were investigated within the frequency range of 10-15 MHz, which is widely used in clinical treatments [30].

The current research aimed to compare the presence and non-presence states of magnetite in order to fabricate four different tumors, including without magnetite nanoparticles, and with the magnetite amounts of 0.01, 0.05, and 0.1 gram. After determining the properties of the phantom, the phantom was placed in an electromagnetic field with the frequency of 13.56 MHz. The main objective of the present study was to compare two states of using and not using magnetite nanoparticles and investigate the effects of magnetite on breast cancer therapies at a frequency band commonly used in clinical devices and treatments.

MATERIALS AND METHODS

This section has been presented in five sub-sections of geometry design, fabrication of the phantom, measurement of thermal and dielectric properties, disposition of the phantom in radiofrequency (RF) radiation, and measurement of the specific absorption rate (SAR).

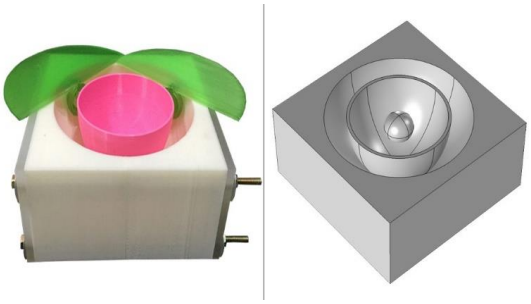

Fig 1. Design of phantom and 3D-printed phantom

Geometry design

At this stage, proper geometry was designed using the SOLIDWORKS software (version 2018 SP5.0) to represent an actual breast. Three different tissues of a cancerous breast were considered in the design process, including the fat, glandular, and tumor tissues. A radius hemisphere (5 cm) was designed in the form of a breast (diameters: 3.5×5 cm) with a semi-oval embedded inside, which represented the glandular tissues, and the distance between the hemisphere and semi-oval represented the fat tissues.

Table 1. Weight of materials in each tissue

Material / Tissues	Oil (gr)	Gelatin (gr)	Water (gr)	Salt (gr)	Surfactant (gr)	Formaldehyde (gr)
Fat	121.49	13.69	35.93	0	6.8	2.16
Gland	24.68	32.81	98.74	0	1.38	1.73
Tumor	1	1.9	5.7	0.18	0.07	0.11

Table 2. Physical properties of magnetite

R (nm)	$C\left(J/kg°C\right)$	$\rho\left(kg/m^3\right)$	$\sigma\left(S.m^{-1}\right)$	$\kappa(w/m°C)$
16.5	670	5180	0.025	9.7

R: Radius, C: Specific heat capacity, : Density, : Electrical Conductivity, : Thermal Conductivity

At the bottom of the semi-oval, a radius sphere (1 cm) was inserted as a tumor. This geometry was eventually utilized using a 3D printer.

Fig 1 depicts the designed and fabricated phantom.

Fabrication of the phantom

The properties of the oil-gelatin phantom are noticeably similar to actual tissues compared to other materials [31]. For instance, agar mixtures have a high melting point (approximately 80˚C), which enables them to preserve their shape, while their permittivity is lower than actual tissues. Therefore, agar mixtures cannot represent the dielectric properties of tissues [32]. TX-150 could be successfully utilized to represent high-water-content tissues (e.g., tumor), while it cannot be used for low-water-content tissues (e.g., fats) [31]. However, oil-gelatin mixtures could be easily prepared homogeneously, and added formaldehyde could maintain their shape at high temperatures. As such, their behavior in an electromagnetic field in hyperthermia could represent actual tissues remarkably more than other materials. In the present study, the main materials used to fabricate the phantom included calfskin gelatin (Sigma-Aldrich, USA), safflower oil, and water. Moreover, the addition of sodium chloride to the mixture helped adjust the electrical conductivity of the tumor tissue. The specific heat capacity of oil is lower than water (the specific heat capacity of oil is approximately 1/64 , while it is 4/42 in water). Therefore, we used water instead of oil for the adjustment of these properties in the tissues with high specific heat capacities, such as the tumor and glandular tissues.

The prepared mixture in the current research contained both hydrophilic and hydrophobic materials. Therefore, sodium lauryl sulfate was used as a surfactant in order to bring homogeneity to the phantom. In order to stabilize the phantom at high temperatures, formaldehyde was added to the mixture to increase its melting point and prevent its transfiguration [17].

Fig 2. Cube used for fabrication of tumor tissues (hole was used for mixture injection)

In order to achieve the least difference in the four studied states and decrease measurement errors, the healthy tissues (glandular and fat) were identical in all the states, so that the properties of the healthy tissues would be equal in all the states. Table 1 shows the weight values of the materials in each tissue. In the fabrication of the phantom, the fat mixture was initially prepared and placed in a region of the phantom that was considered as the fat layer. In accordance with the method proposed by Lazebnik et al., the formaldehyde cross-linking of gelatin was completed within a minimum of five days [17].

Afterwards, the gland mixture was prepared, and after five days, the phantom was divided into two parts for the placement of the tumor inside. To make the tumor completely spherical with the radius of one centimeter, a cube composed of a spherical hole with the radius of one centimeter was used (Fig 2). Finally, various weights of magnetite were added to the tumor region (0.01, 0.05, and 0.1 g).

Magnetite (Fe_3O_4) nanoparticles were prepared

using the chemical co-precipitation method in 80˚C with sodiumcitrate and oleic acid as modifiers [33], and X-ray diffraction (XRD) was applied to determine the crystal structure of magnetite (Fig 3).

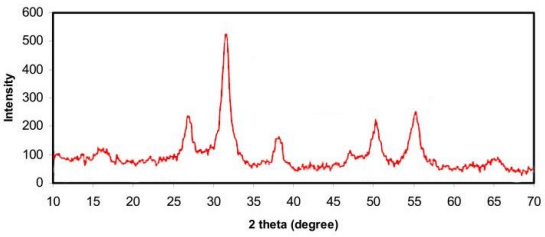

Fig 3. XRD pattern of Magnetite (Fe3O4) MNPs

In addition, transmission electron microscopy (TEM) imaging was used to measure the mean radius of magnetite, which was estimated at 16.5 nanometers (Fig 4). The physical properties of Fe_3O_4 are presented in Table 2. In the current research, we evaluated four types of tumors (no magnetite and with three weights of magnetite). Fig 5 illustrates the final phantom after fabrication.

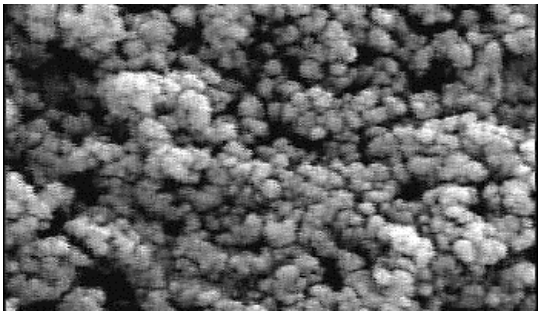

Fig 4. TEM image of Fe3O4 nanoparticles (mean: 16.5 nm)

Fig 5. Oil-gelatin phantom of breast with fat, glandular, and tumor tissues

Measurement of the thermal and dielectric properties

After the fabrication of the phantom, the thermal and dielectric properties of the phantom were determined and compared to actual breast tissues. In order to determine the thermal properties (specific heat capacity, thermal conductivity, and density), nine samples were obtained from various parts of each tissue to improve the measurement accuracy, and their amounts were measured using a calorimeter. Table 3 shows the measured thermal properties.

Table 3. Values of Thermal Properties in Each Tissue of Phantom with Actual Values of Breast Tissues

Tissues		Fat	Gland	Tumor
Specific heat capacity $(j/kg℃)$	Real amount	2280	3639	3639
	Measure amount	2300	3670.5	3670.5
Thermal conductivity $(w/m℃)$	Real amount	0.3	0.56	0.56
	Measure amount	0.3	0.56	0.56
Density (kg/m^3)	Real amount	1069	1050	1050
	Measure amount	1070	1048	1048

In general, the most prominent dielectric properties were relative permittivity and conductivity. Permittivity is defined as a complex physical quantity consisting of an actual part and a hypothetical part. The actual part is the ability of a medium to store the electric field energy, and the hypothetical part is defined as a loss factor that describes the dissipated energy in the material [31]. In the present study, the complex permittivity was determined using Equation 1, as follows:

$$\varepsilon = \varepsilon' - j\varepsilon'' \quad (1)$$

where ε , ε', and ε'' denote the complex permittivity, the actual part of permittivity, and the hypothetical part of permittivity (loss factor), respectively.In the current research, the permittivity calculations in the complex form were extremely difficult. Therefore, we used some simplifications and capacitor concepts. According to the capacitor equations, the air-to-medium capacity of the capacitor described the complex permittivity and normalized permittivity of the tissues based on the vacuum representing the relative permittivity. Equations 2 and 3 were used to calculate the relative permittivity and conductivity relations, respectively.

$$\varepsilon_r = \frac{C}{K} \quad (2)$$

$$\sigma = \frac{G\varepsilon_0}{K} \quad (3)$$

In the equations above, *C*, *K*, , and *G* represent the capacitance of the capacitor in the tissues, capacitance of the capacitor in the air, permittivity of the free space, and conductivity of the capacitor, respectively. Table 4 shows the dielectric properties of the fabricated phantom.

Table 4. Values of Dielectric Properties in Each Tissue of Phantom

Tissues	Fat	Gland	Tumor
Relative permittivity ε_r	11.8	138.4	142.5
Electrical conductivity $\sigma(S.m^{-1})$	0.03	0.63	0.71

Disposition of the phantom in RF radiation

After the measurement of the thermal and dielectric properties, the phantom was disposed in an RF field using the Celsius TCS device (Celsius 42+ GmbH, Cologne, Germany) with the frequency of 13.56 MHz (Fig 7-a). The device is composed of two pairs of electrodes in two sizes of 15 and 25 centimeters (Fig 7-b), which are located on the top and at the bottom of the phantom. The shape of the electromagnetic field between the two electrodes is depicted in Fig 6.

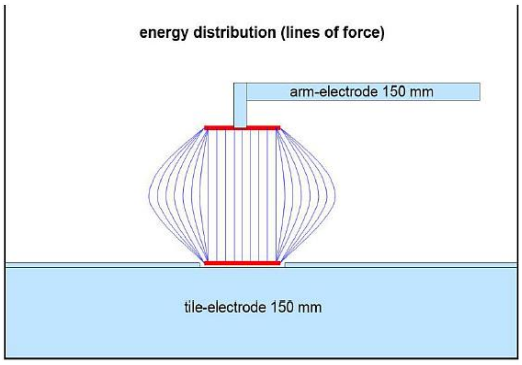

Fig 6. Energy distribution (lines of force; 150-mm electrode on top and 150-mm electrode at bottom)

SAR measurement

SAR is the rate at which the human body tissues absorb energy when an external force is applied. The external force is the energy that is generated by an electric field, electromagnetic waves or ultrasound waves.

In the present study, SAR was defined as the amount of the heat generated by the electromagnetic waves measured (W/m^3) [25].

Since the only heat source and heat absorber were the electromagnetic field and phantom, respectively, SAR was considered to be the heat generation. The SAR at several points of the phantom was calculated using Equation 4, as follows:

$$SAR(w\ /\ m^3) = \rho c \left.\frac{dT}{dt}\right|_{t=0} \quad (4)$$

RESULTS AND DISCUSSION

In the present study, using electrodes with the same size at each side resulted in focusing at the central point, where the maximum intensity was achieved.

Therefore, the tumor was adjusted at this point in order to prevent the extra heating of the healthy tissues, particularly the fat tissues, due to their low specific heat capacity. Fig 7-c shows the phantom between the two electrodes.

The measurement of temperature at specific points of the phantom was performed using a thermocouple (model: Extech 421509).

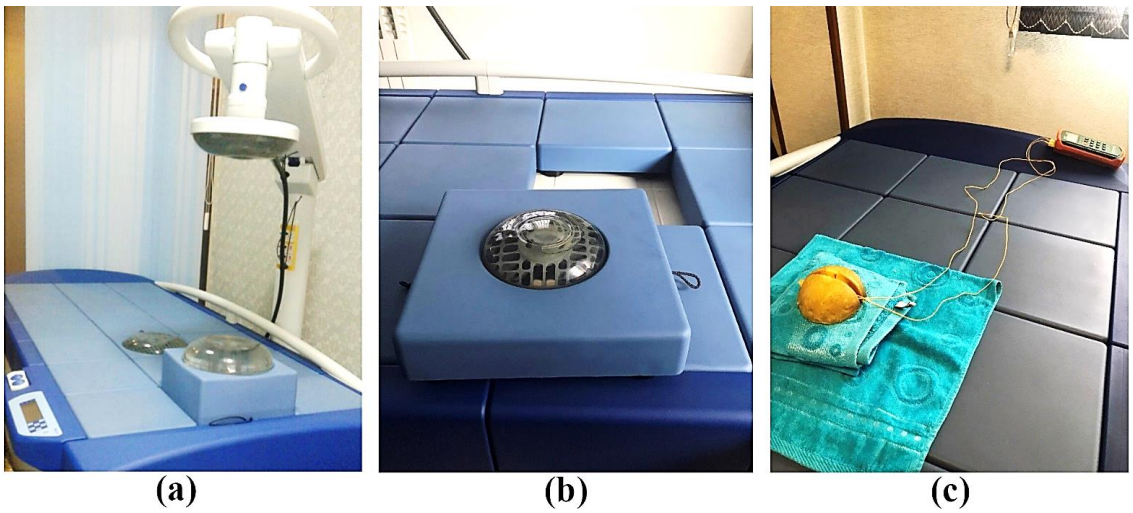

Fig 7. RF Hyperthermia Device; a) Celsius TCS (Celsius 42+ GmbH, Cologne, Germany); b) Bottom Electrode of Device (150 mm); c) Phantom on Hyperthermia Device (Phantom shifted up to adjust tumor on focus point)

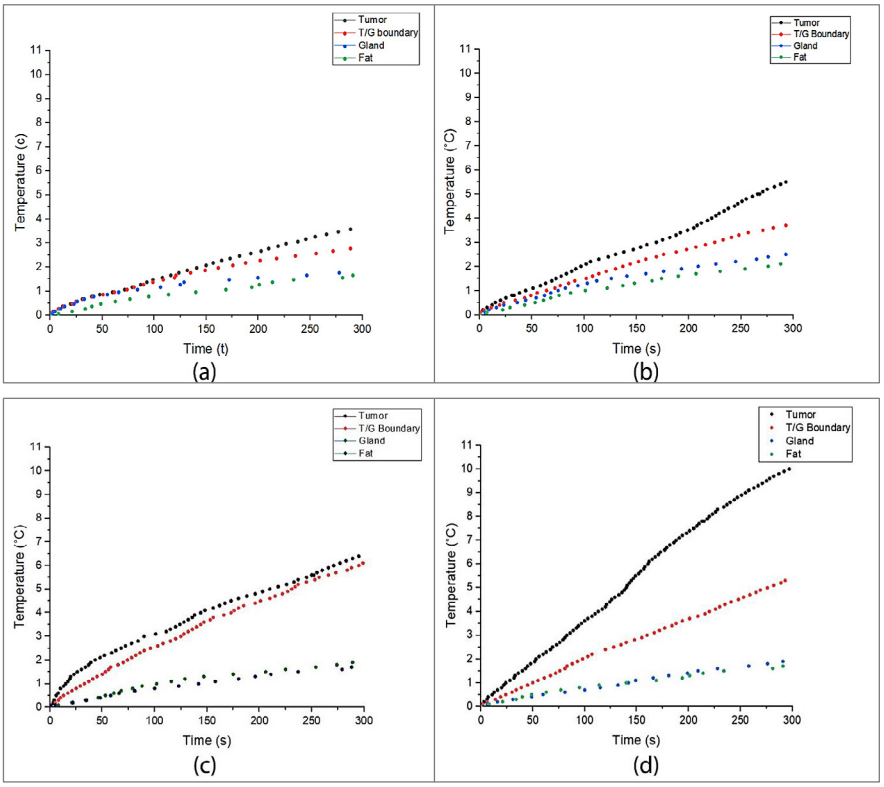

Fig 8. Increasing of temperature in several points of phantom in all states (T/G boundary point as boundary between tumor and glandular tissues); a) Non-presence state of magnetite; b) State with 0.01 gram of magnetite; c) State with 0.05 gram of magnetite and d) state with 0.1 gram of magnetite

Fig 8 shows the mean temperature after five replicates of each state. Each point in Fig 8 was achieved directly, and the temperature difference of 0.1˚C was recorded. In addition, several powers and times were investigated with both sizes of the electrodes so as to determine the proper parameters.

After multiple tests, the proper power and time for the breast tissues at the mentioned frequency were determined to be 40 watts and five minutes, respectively. In the non-presence state of magnetite, the temperature of the tumor from its center to its border was within the range of 3-3.6˚C, while the temperature in the glandular and fat tissues was estimated at 1.8˚C and 1.6˚C, respectively. In the state with 0.01 gram of magnetite, the temperature of the tumor from its center to its border was within the range of 5.5-3.7˚C, while in the glandular and fat tissues, this value was estimated at 2.5˚C and 2.1˚C, respectively. In the state with 0.05 gram of magnetite, the temperature of the tumor from its center to its border was within the range of 6.4-6.1˚C, while the temperature of the glandular and fat tissues was estimated at 1.9˚C and 1.7˚C, respectively. In the state with 0.1 gram of magnetite, the temperature of the tumor from its center to its border was within the range of 10-5.3˚C, while the temperature of the glandular and fat tissues was estimated at 1.9˚C and 1.7˚C, respectively.

As is depicted in Fig 9, at the early stages of the treatment, the temperature values obtained in all the states from the center to the border of the tumor were close. However, the increasing of the time resulted in the decreased heat transfer from the center to the border, while the temperature difference between the two points increased.

In the presence state of magnetite, the temperature of the tumor center was adequately high to cause ablation in this region. However, Fig 9 shows that the heat distribution from the center to the border of the tumor region in the states with 0.01 and 0.1 gram of magnetite was not sufficiently high to cause damage in the entire tumor region.

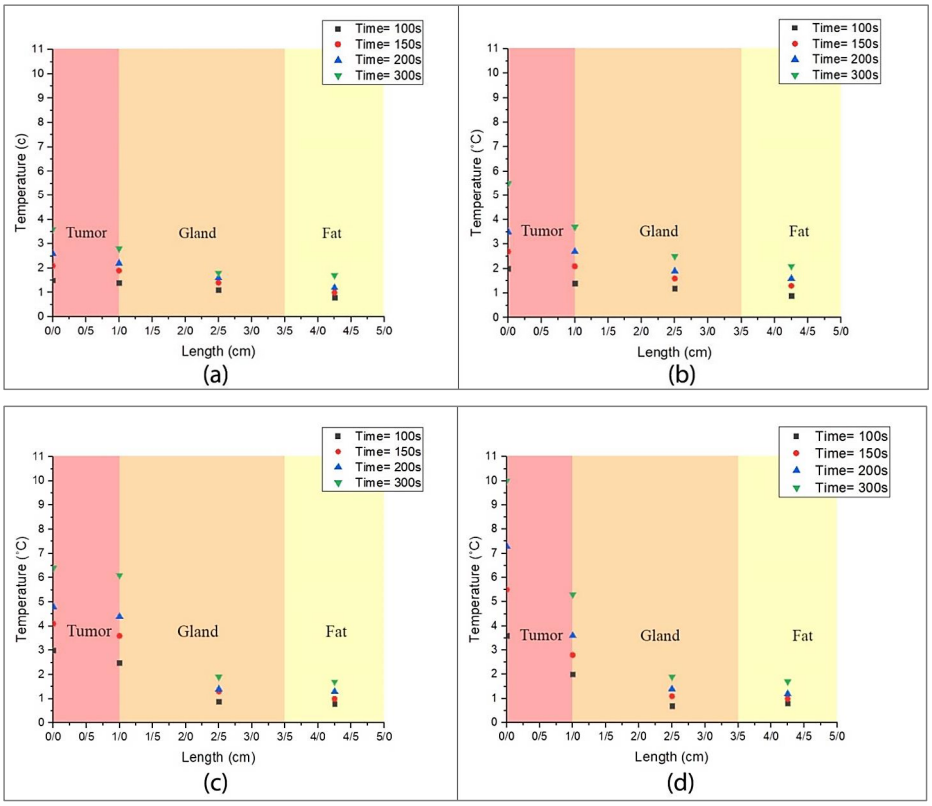

Fig 9. Temperature of each tissue at four different times in all states; a) Non-presence state of magnetite, b) state with 0.01 gram of magnetite, c) state with 0.05 gram of magnetite; and d) State with 0.1 gram of magnetite

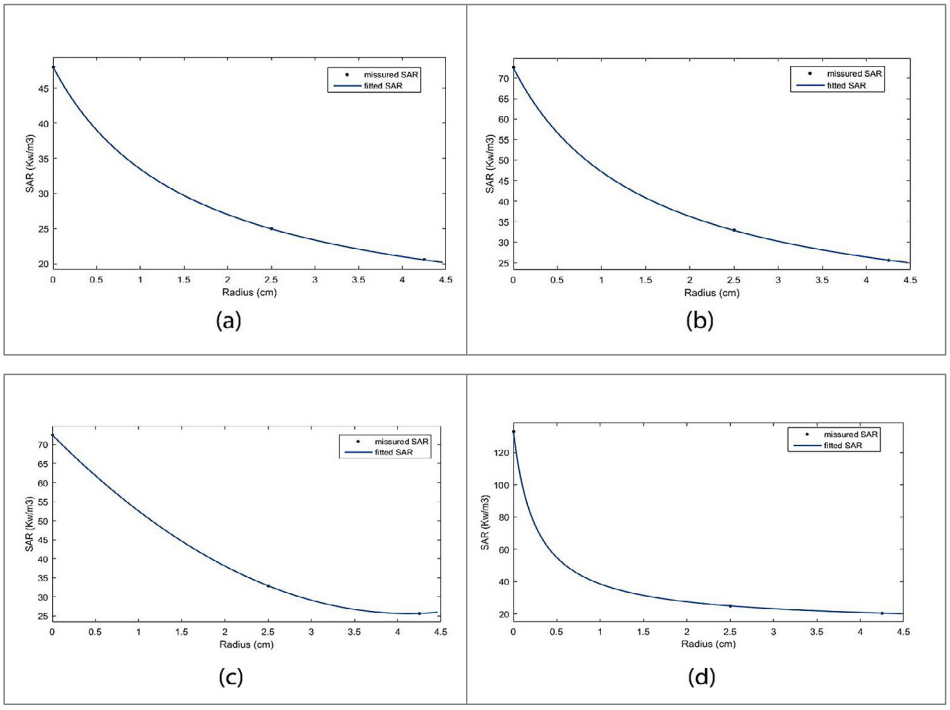

Fig 10. SAR distribution on phantom for five minutes in all states; a) Non-presence state of magnetite, b) state with 0.01 gram of magnetite, c) state with 0.05 gram of magnetite, and d) state with 0.1 gram of magnetite

Therefore, equal heat could not be tolerated by the entire tumor region in these states. However, in the state with 0.05 gram of magnetite, equal heat could be tolerated in the center to the border of the tumor region.

In the current research, Equation 4 was used to calculate the SAR of all the states, and the amount of energy that was absorbed in each state during treatment was obtained as well. The total SAR of each phantom is shown in Fig 10. As can be seen, the total SAR in the phantom was inversely correlated with the radius due to the properties of the tissues and focusing. In addition, the high conductivity of the tumor specifically increased the absorption rate and heat generation in this region.

CONCLUSION

In the present study, a homogenous breast phantom was fabricated for RF hyperthermia studies with the frequency of 13.56 MHz, which is commonly used in clinical treatments. Most of the studies in this regard have used the frequency bands that are not generally applied in clinical treatments with other RF sources than clinical devices. In earlier studies, only the mimicking of a phantom was considered important. In most of the researches in this regard, the effects of magnetite on a gel combination at various concentrations have not been thoroughly investigated. In our previous study, we assessed a proper mixture that was more similar to an actual breast compared to other mixtures. According to the current research, the temperature of the tumor increased by approximately 3-3.6˚C, while the increasing of temperature by at least 6˚C is considered essential to achieving significant effects on the success rate of breast cancer treatment. Since breast tissues contain fats, and the specific heat capacity of fat is lower than other parts, it is crucial to have an exact focus point and use power and time in order to prevent damage to these tissues. Consequently, the increasing of the power and time of treatment is impossible. In order to achieve adequate influence on the tumor region in the present study, magnetic nanoparticles were used to cause more ablation.

In order to investigate the effects of magnetite, three different weights of magnetite were prepared in this study. After measuring important parameters and ensuring that the designed phantom was able to represent an actual cancerous breast, the phantom was placed in an electromagnetic field, which has numerous clinical applications in cancer treatment. The behavior of the phantom at the RF of 13.56 MHz using the hyperthermia device indicated the extreme temperature rise in the tumor tissues in all the states, causing no damage to the healthy tissues. Furthermore, the measurement of the increased temperature at various points and calculation of the SAR in all the states demonstrated that in the state with 0.05 gram of magnetite, heat distribution was adequate to cause damage to the cancerous breast tissue at the mentioned frequency using the device.

AKNOWLEDGMENTS

This article has been extracted from the thesis written by Mrs. Mahsa Kavousi at school of medicine, Tehran University of Medical Science.

REFERENCES

1. González-Díaz C, Uscanga-Carmona MC, Ibarra-Martínez CD, Jiménez-Fernández ME, Lozano Trenado LM, Silva-Escobedo JG, Polo-Soto SM. Differentiation BIRADS I vs II by Magnetic Induction Spectroscopy: A Potential Innovative Method to Detect Neoplasies in Breast. Revista Mexicana de Ingeniería Biomédica. 2012; 33(2): 65-76.
2. Mannello F. Understanding breast cancer stem cell heterogeneity: time to move on to a new research paradigm. BMC Medicine. 2013; 11(1): 169.
3. Velasco-Velázquez M A, Homsi Nora, De La Fuente Marisol, Pestell Richard G. Breast cancer stem cells. Int J Biochem Cell Biol. 2012; 44(4): 573-577.
4. Al-Hajj Muhammad, Wicha Max S, Benito-Hernandez Adalberto, Morrison Sean J, Clarke Michael F. Prospective identification of tumorigenic breast cancer cells. Proc Natl Acad Sci. U.S.A. 2003; 100(7): 3983-3988.
5. Jordan A, Wust P, Scholz R, Tesche B, Fähling H, Mitrovics T, Vogl T, Cervos-Navarro J, Felix R. Cellular uptake of magnetic fluid particles and their effects on human adenocarcinoma cells exposed to AC magnetic fields in vitro. Int J Hyperth. 1996; 12(6): 705-722.
6. Nielsen OS, Horsman M, Overgaard J. A future for hyperthermia in cancer treatment?. Eur J Cancer. 2001; 37(13): 1587-1589.
7. Sneed PK, Stauffer PR, McDermott MW, Diederich CJ, Lamborn KR, Prados MD, Chang S, Weaver KA, Spry L, Malec MK, Lamb SA, Voss B, Davis RL, Wara WM, Larson DA, Phillips TL, Gutin PH. Survival benefit of hyperthermia in a prospective randomized trial of brachytherapy boost ± hyperthermia for glioblastoma multiforme. Int J Radiat Oncol. 1998; 40(2): 287-295.
8. Lee TW, Murad Greg JA, Hoh BL, Rahman M. Fighting Fire with Fire: The Revival of Thermotherapy for Gliomas. Anticancer Res. 2014; 34(2): 565-574.
9. Carpentier A, McNichols RJ, Stafford RJ, Guichard J-P, Reizine D, Delaloge S, Vicaut E, Payen D, Gowda A, George B. Laser thermal therapy: Real-time MRI-guided

and computer-controlled procedures for metastatic brain tumors. Lasers Surg Med. 2011; 43(10): 943-950.
10.Sneed, P.K., Hyperthermia. Textbook of Radiat Oncol. 2004; :1569-1596.
11.Wust P, Hildebrandt B, Sreenivasa G, Rau B, Gellermann J, Riess H, Felix R, Schlag PM. Hyperthermia in combined treatment of cancer. Lancet Oncol. 2002; 3(8): 487-497.
12.Falk MH, Issels RD. Hyperthermia in oncology. Int J Hyperth. 2001; 17(1): 1-18.
13.Horsman M, Overgaard J. Hot Topic: Can mild hyperthermia improve tumour oxygenation?. Int J Hyperth. 1997; 13(2): 141-147.
14.Henrich F, Rahn H, Odenbach S. Heat transition during magnetic heating treatment: Study with tissue models and simulation. J Magn Magn Mater. 2015; 380: 353-359.
15.Gilchrist RK, Medal R, Shorey WD, Hanselman RC, Parrott JC, Taylor CB. Selective inductive heating of lymph nodes. Ann Surg. 1957; 146(4): 596-606.
16.Stang J, Haynes M, Carson P, Moghaddam M. A preclinical system prototype for focused microwave thermal therapy of the breast. IEEE Trans Biomed Eng. 2012; 59(9): 2431-2438.
17.Lazebnik M, Madsen EL, Frank GR, Hagness SC. Tissue-mimicking phantom materials for narrowband and ultrawideband microwave applications. Phys Med Biol. 2005; 50(18): 4245-4258.
18.Mukherjee S, Udpa L, Udpa S, Rothwell EJ, Deng Y. Microwave Time-Reversal Mirror for Imaging and Hyperthermia Treatment of Breast Tumors. Prog Electromagn Res. 2019; 77: 1-16.
19.Yuan Y, Wyatt C, Maccarini P, Stauffer P, Craciunescu O, MacFall J, Dewhirst M, Das SK. A heterogeneous human tissue mimicking phantom for RF heating and MRI thermal monitoring verification. Phys Med Biol. 2012; 57(7): 2021.
20.Miaskowski A, Sawicki B. Magnetic fluid hyperthermia modeling based on phantom measurements and realistic breast model. IEEE Trans Biomed Eng. 2013; 60(7): 1806-1813.
21.Tayel M, Abouelnaga T, Elnagar A. Pencil Beam Grid Antenna Array for Hyperthermia Breast Cancer Treatment System. Circ Syst. 2017; 8(05): 122.
22.Nguyen PT, Abbosh AM, Crozier S. Thermo-Dielectric Breast Phantom for Experimental Studies of Microwave Hyperthermia. IEEE Antennas Wirel Propag Lett. 2016; 15: 476-479.
23.Hergt R, Dutz S, Müller R, Zeisberger M. Magnetic particle hyperthermia: nanoparticle magnetism and materials development for cancer therapy. J Phys Condens Matter. 2006; 18(38): 2919.
24.Jeun M. Physical limits of pure superparamagnetic Fe3O4 nanoparticles for a local hyperthermia agent in nanomedicine. Appl Phys Lett. 2012; 100(9): 092406.
25.Heydari M, Javidi M, Attar MM, Karimi A, Navidbakhsh M, Haghpanahi M, Amanpour S. Magnetic fluid hyperthermia in a cylindrical gel contains water flow. J Mech Med Biol. 2015; 15(05): 1550088.
26.Henrich F, Rahn H, Odenbach S. Investigation of heat distribution during magnetic heating treatment using a polyurethane–ferrofluid phantom-model. J Magn Magn Mater. 2014; 351: 1-7.
27.Ma M, Zhang Y, Shen X, Xie J, Li Y, Gu N. Targeted inductive heating of nanomagnets by a combination of alternating current (AC) and static magnetic fields. Nano Res. 2015; 8(2): 600-610.
28.Kappiyoor R, Liangruksa M, Ganguly R, Puri IK. The effects of magnetic nanoparticle properties on magnetic fluid hyperthermia. J Appl Phys. 2010; 108(9): 094702.
29.Joines WT, Zhang Y, Li C, Jirtle RL. The measured electrical properties of normal and malignant human tissues from 50 to 900. Med Phys. 1994; 21(4): 547-550.
30.Kavousi M, Saadatmand E, Riahi Alam N. Physical Parameters Measurement of Breast Equivalent Phantom for Clinical Studies in Radiofrequency Hyperthermia. Frontiers Biomed Technol. 6(1):28-34.
31.Dabbagh A, Abdullah AJJ, Ramasindarum C, Abu Kasim NH. Tissue-Mimicking Gel Phantoms for Thermal Therapy Studies. Ultrason Imaging. 2014; 36(4): 291-316.
32.Zhou T, Meaney PM, Fanning MW, Geimer ShD, Paulsen KD. Integrated microwave thermal imaging system with mechanically steerable HIFU therapy device. Spie Bios. 2009; 7181.
33.Wei Y, Han B, Hu X, Lin Y, Wang X, Deng X. Synthesis of Fe3O4 nanoparticles and their magnetic properties. Procedia. 2012; 27: 632-7.